

Short communication

NIR-responsive transdermal delivery of atenolol based on polyacrylamide-modified MoS₂ nanoparticles

Kai Zhang^a, Ying Zhao^b, Linlin Wang^a, Lili Zhao^a, Xiaochang Liu^{c,d,*}, Shaoheng He^{d,*}

^a College of Science and Technology, Hebei Agricultural University, Cangzhou, China

^b Department of Pharmacy, Shaanxi Provincial People's Hospital, Xi'an, China

^c School of Pharmacy, Shenyang Medical College, Shenyang, China

^d Translational Medicine Research Centre, Shenyang Medical College, Shenyang, China

ARTICLE INFO

Keywords:

TDDS
Photothermal conversion
Drug loading
Controlled release
Polyacrylamide-modified molybdenum disulfide

ABSTRACT

Transdermal drug delivery system (TDDS) is a successful non-invasive drug delivery system that shows several advantages. However, dose depletion effects remain a major challenge for sustained release TDDS. This study aimed to develop a polyacrylamide-modified MoS₂ nanoparticles (CPAM-MoS₂ NPs) based TDDS, which could control drug release and prolong the treatment time by light stimulation. In this work, the CPAM-MoS₂ were produced by a facile hydrothermal method. The structure of CPAM-MoS₂ NPs was detected by using FTIR, XRD and TEM, and the surface morphology of the NPs was observed by SEM. The colloid stability was tested by zeta potential and sedimentation volume ratio. Moreover, *In vivo* skin erythema study was conducted to explore the biocompatibility of CPAM-MoS₂ NPs. As a result, the synthesized colloid-stable and skin-safe CPAM-MoS₂ NPs possessed a high drug load efficiency of 87.2% and excellent photothermal conversion efficiency that was successfully applied in a TDDS with an enhancement ratio of 1.82. We measured its controlled release ability in an *in vitro* skin penetration test and, moreover, no drug depletion was observed during the 8-hour study in the light stimulation group. This paper describes the first use of CPAM-MoS₂ NPs as a carrier for drugs in a TDDS.

1. Introduction

Transdermal drug delivery system (TDDS) is a successful non-invasive drug delivery system that shows outstanding performance in increasing patient compliance, decreasing side effects, and avoiding the first-pass effect [1–4]. Skin is a natural barrier for the transdermal administration of many chronic diseases [5,6]. The numerous studies and increasing number of transdermal products have demonstrated the potentials of TDDS applications [7]. However, despite its great potential, dose depletion effects have hindered the development of TDDS [8].

Recent developments in materials science and nanotechnology have led to the adoption of various emerging materials in drug delivery applications [9,10]. Inorganic nanomaterials have gained significant interest in research and have been widely used in controlled release systems, because not only does inorganic nanomaterials possess high drug loading efficiency but also, more importantly they are very biocompatible [11–13]. Additional stimulation is typically required in most inorganic nanomaterial drug delivery systems, where stimuli may include pH, electrical, light, and electrochemical change [14–16]. Light-

stimulated materials that exhibit photothermal conversion ability have been used in cancer treatments, such as graphene oxide, Au-/Pd-based nanomaterials, and MoS₂ et al. [17–21].

While various inorganic nanomaterials have been investigated in previous studies, emerging MoS₂ materials and their derivatives have gained popularity due to their extraordinary photothermal conversion effect [22–25]. Chou et al. provided the first demonstration of the superior photothermal conversion ability of exfoliated MoS₂ nanosheets in comparison with Au-based nanorods and graphene [21]. Liu et al. developed a multifunctional drug delivery system based on PEGylated MoS₂ that exhibited excellent anti-tumor effects in both lung cancer cells and animal experiments [26]. Yang et al. investigated colloidal stable MoS₂ nanoparticles functionalized with polyvinyl pyrrolidone that exhibited a high drug loading capacity and controlled release of the model drug [24]. Unfortunately, the problems associated with metabolism *in vivo* are rarely addressed in previous studies, which is a glaring challenge for the practical application of MoS₂ and its derivative materials.

This study aimed to develop a novel MoS₂-based atenolol (ATE)

* Corresponding authors at: School of Pharmacy, Shenyang Medical College, Shenyang, China (X. Liu).

E-mail addresses: liuxiaochang1991@163.com (X. Liu), hbxazk@163.com (S. He).

<https://doi.org/10.1016/j.inoche.2020.108277>

Received 27 August 2020; Received in revised form 24 September 2020; Accepted 25 September 2020

Available online 28 September 2020

1387-7003/© 2020 Elsevier B.V. All rights reserved.

TDDS for the treatment of hypertension. Controlled release of the model drug ATE was achieved due to the light-stimulated properties of the material, while the high drug loading capacity of MoS₂ was expected to resolve the dose depletion issues typically associated with TDDS. On the other hand, the specialized transdermal administration had the potential to circumvent the toxicity of MoS₂ by preventing MoS₂ across the skin. Polyacrylamide-modified MoS₂ nanoparticles (CPAM-MoS₂ NPs) were synthesized and further characterized. In order to provide insight for further clinical application of CPAM-MoS₂ NPs, the controlled-release ability, a key parameter of controlled release preparations, was also tested *in vitro*.

2. Materials and methods

2.1. Materials

Sodium molybdate dihydrate (Na₂MoO₄·2H₂O) and thiourea (CH₄N₂S) were purchased from Tianjin Kemiou Chemical Reagent Co. Ltd (Tianjin, China). Cationic polyacrylamides (CPAM, Mw = 8000000 g/mol) were obtained from Tianjin Damao Chemical Reagent Factory (Tianjin, China). Atenolol (98%) was acquired from Tianjin Heowns Biochemical Technology Co., Ltd. (Tianjin, China). All chemicals were used as received. The deionized water (18.2 MΩ) used throughout the studies was supplied by Milli-Q system (Millipore, USA).

2.2. Synthesis of CPAM-MoS₂ NPs

The synthesis of flowerlike MoS₂ NPs was carried out by a simple, facile hydrothermal method. In brief, 1.24 g Na₂MoO₄·2H₂O was first added to 36 mL of deionized water, then 2.28 g CH₄N₂S was added under vigorously magnetic stirring. After 30 min of continuous stirring, the obtained solution was enclosed into Teflon-lined stainless-steel autoclave and sealed tightly, heated at 220 °C for 6 h in an electric oven and naturally cooled to ambient temperature. Black precipitates were purified by centrifugation and washing with water and ethanol respectively. After drying at 45 °C for 24 h in air, the resulting product was kept at 4 °C for further use.

The flowerlike CPAM-MoS₂ NPs were prepared as follows: 1.0 g flowerlike MoS₂ NPs was dispersed in 200 mL CPAM solution (0.5 wt%) in a flask under stirring. The mixture was ultrasonic for 1 h and stirred at 80 °C for 4 h. The resultant black precipitate was collected by centrifugation and subsequently purified by washing with water and ethanol for several times, and dried at 45 °C for 24 h in air.

2.3. Characterization of CPAM-MoS₂ NPs

The surface functional group of CPAM-MoS₂ NPs was characterized by Fourier transform infrared (FTIR Perkin Elmer 2000) spectroscopy with KBr as background. X-ray diffraction (XRD, Rigaku SmartLab) characterization was applied to investigate the crystal phases of the as-synthesized samples. The surface morphology of the samples was observed by using a scanning electron microscope (SEM, Hitachi SU8100) with an energy dispersive spectroscopy (EDS) unit. Transmission electron microscopy (TEM, JEOL JEM-2100F) measurements were performed at 200 kV. The colloidal stability was analyzed by zeta potential and sedimentation volume ratio. Zeta potential was analyzed by dynamic light scattering (DLS, Melvin 2000). The sedimentation volume ratio was determined by the ratio of the height after (H_u) and before (H₀) the sedimentation.

2.4. *In vivo* skin erythema index test

A Mexameter® instrument (C&K Co., Germany) was introduced to obtain erythema index of the rabbit's skin. Four separate parts with an area of 2.5 × 2.5 cm of the side of the abdomen of the rabbits was carefully shaved. *EI* value (*EI*₀) of each part of the skins was measure

after the skin was gently cleaned with water. 10% (w/v) sodium dodecyl sulfate (SDS) water solution as the positive control and PBS was used as the control for the CPAM-MoS₂ NPs (0.5 mg/mL) with 5 min NIR-irritation. 500 μL of irritations were applied onto the skin. After 8 h, the skin was cleaned with water and the erythema index was measured (*EI*_t). The index Δ*EI* were calculated by subtracting *EI*₀ from *EI*_t.

2.5. Photothermal conversion performance

UV-vis spectra of MoS₂ and CPAM-MoS₂ were tested with a UV-vis spectrophotometer (UV-2600, Shimadzu). A multimode pump laser with a wavelength of 808 nm laser (F34-808ADX, Hashang Laser) was used to test the photothermal conversion performance of CPAM-MoS₂ NPs. Water was studied as control. The effect of NPs concentration (0.1 mg/mL, 0.5 mg/mL and 1.0 mg/mL) and laser density (0.2 W/cm², 0.5 W/cm² and 1.0 W/cm²) on the photothermal conversion performance was monitored with a magnetic stirrer equipped with a temperature monitor. The temperature of the solutions was tested for three on-off cycles to determine the photothermal stability.

2.6. Drug loading

Drug loading was conducted by adding the drug and CPAM-MoS₂ NPs in phosphate buffer saline with a pH of 7.0. The suspension was vigorously magnetic stirring for 2 h and shaken at 32 °C for 24 h. The free drug was removed by centrifugation and the drug-loaded CPAM-MoS₂ NPs was washed clean with water and further dried with an oven at 60 °C. The drug loaded in the MoS₂ NPs was calculated by the concentration of free atenolol which can be determined with the HPLC-UV method described in 2.8.

2.7. *In vitro* drug release study

Horizontal two-chamber diffusion cells were used in *in vitro* drug release study. The effective area and the volume of the diffusion cells were 1.5 cm² and 4 mL, respectively. The temperature was set as 32 °C. A nylon filter membrane with a size of 0.22 μm was used to separate the receptor and the donor cells. 15% PEG400 phosphate buffer solution (PBS, pH 7.4) was added in the receptor cells. Samples of 2.0 mL receptor solution were picked at 1, 2, 3, 4, 5, 6, 7 and 8 h. Fresh acceptor solution of same volume was added every sampling. Light stimulation (0.5 W/cm²) was played for 5 min after the sampling at 1, 3, 5 and 7 h. The samples were analyzed by the method described in 2.8.

Higuchi equation was usually used to describe drug release behavior. A simplified equation was chosen as follows [27]:

$$R = 200 \frac{Dt^{1/2}}{\pi h^2} \approx k\sqrt{t} \quad (1)$$

where *R* was release kinetic constant, *D* was the diffusion rate, *h* was diffusion length and *k* was release rate.

2.8. *In vitro* skin permeation study

Full-thickness skin was mounted between acceptor and donor solutions [28]. All the procedures of skin penetration experiments were similar with drug release study. The differences between the two experiment were that the sampling times (2, 4, 6, 8 h) and the using frequency of laser stimulating (every time after sampling). Skin permeation samples was also determined with HPLC-UV method. The animal experiments were in conformity to the NIH Guidelines for the Care and Use of Laboratory Animals and were approved by the Animal Ethics Committee of Shenyang Medical College.

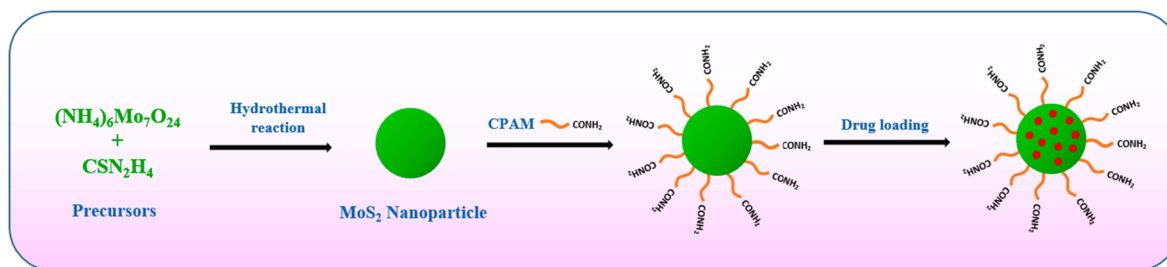


Fig. 1. The use of CPAM-MoS₂ NPs as a carrier capable to deliver ATE.

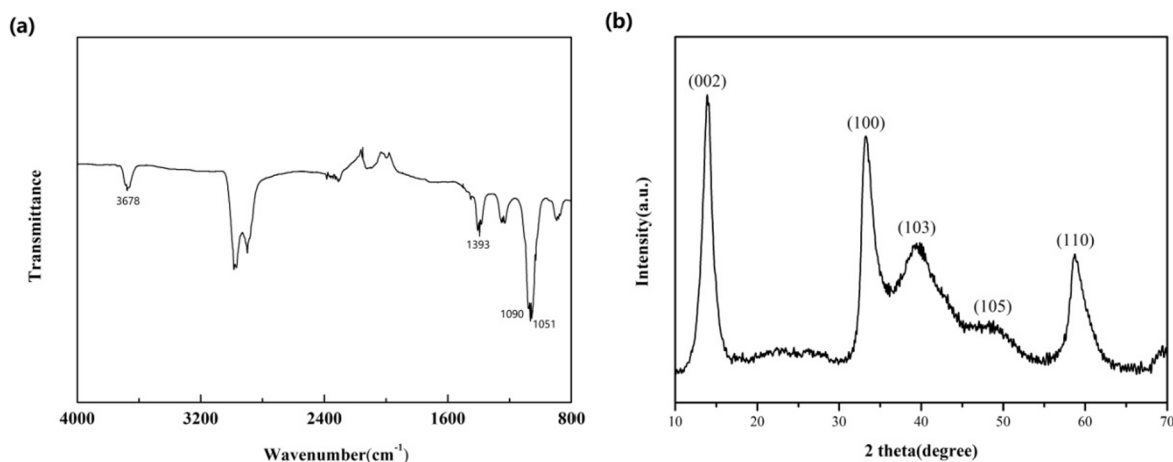


Fig. 2. (a) FTIR spectra of CPAM-MoS₂ NPs. (b) XRD pattern of CPAM-MoS₂ NPs.

2.9. HPLC analysis of the drug

The concentration of atenolol was quantified by HPLC (Hitachi, Tokyo, Japan), which consisted of Pump L-2130, Auto Sampler L-2200 and UV-detector L-2420 and Waters C18 reversed-phase column (200 × 4.6 mm, 5 μm, ODS-2 Waters, America). Methanol, water and phosphoric acid solution (70:30:0.1, v/v) was used to separate the drug

and interferences. Temperature of the column oven was set at 25 °C and the flow rate was set as 0.7 mL/min. The wavelength of detector was set at 275 nm. The analysis method was validated to be rational.

2.10. Statistical analysis

Results were expressed as mean ± S.D. The data were subjected to

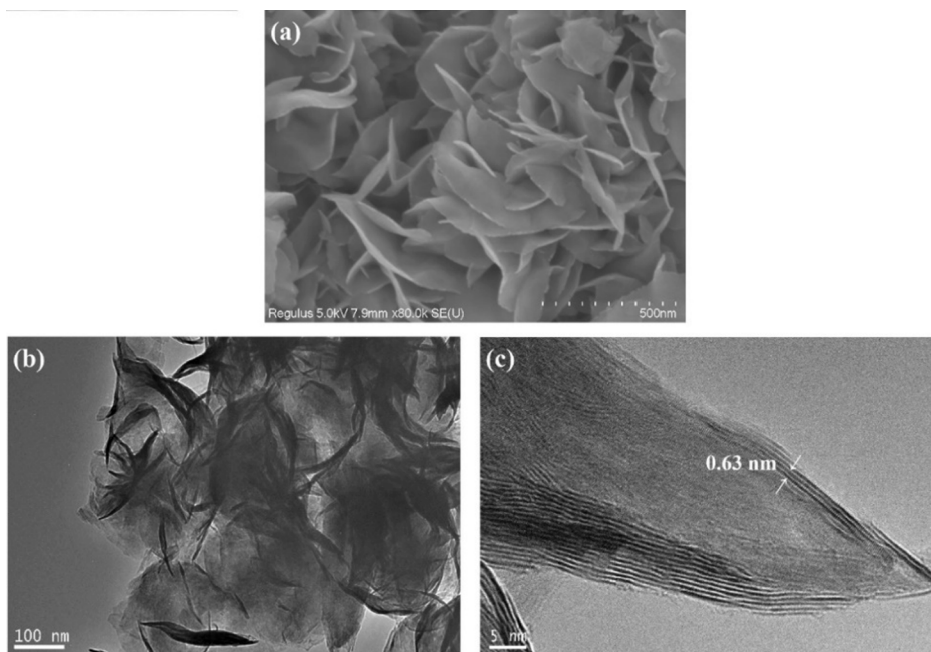


Fig. 3. The (a) SEM, (b) TEM, and (c) HRTEM images of the CPAM-MoS₂ NPs.

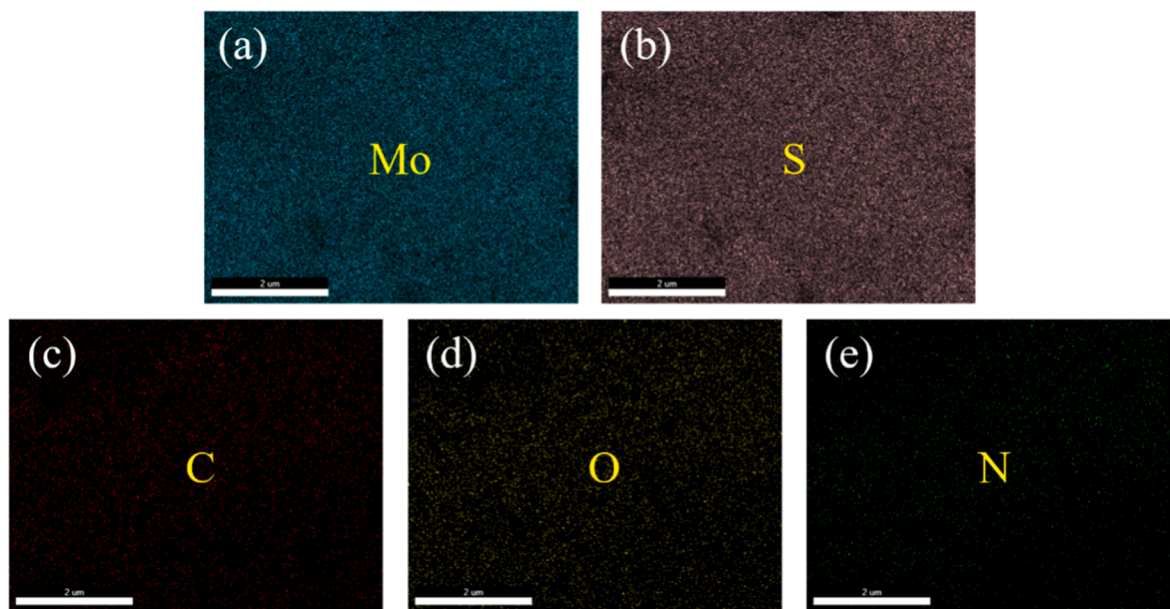


Fig. 4. Elemental mapping images of CPAM-MoS₂ composites: (A) Mo element, (B) S element, (C) C element, (D) O element, (e) N element.

analysis of variance (ANOVA) using SPSS 16.0 software. A significant level was taken as $p < 0.05$.

3. Results and discussion

3.1. Synthesis and characterization of CPAM-MoS₂ NPs

The flower-like MoS₂ NPs surface modified with CPAM were produced by a simple, facile hydrothermal method. This method has been reported in previous literature, where MoS₂ was decorated with poly(ethylene glycol) for traceable and pH-responsive chemotherapeutic drug delivery [29]. The CPAM-MoS₂ NPs synthesis procedure was shown in Fig. 1. CPAM is widely applied in biomedical applications and was used as a modifier due to its great hydrophilicity and non-toxicity [30–33].

The CPAM surface modification of MoS₂ was monitored using FTIR. The spectra of CPAM-MoS₂ NPs in Fig. 2a. The peaks at 3678 cm⁻¹ and 1393 cm⁻¹ attributed to N–H stretching vibrations and C–N stretching vibrations, respectively. The peaks at 1051 cm⁻¹ and 1090 cm⁻¹ were the characteristic peaks of MoS₂ [24]. These observations indicated successful surface modification of MoS₂ with CPAM.

The crystallinity and structure of the samples were evaluated using XRD. The flower-like CPAM-MoS₂ NPs exhibited peaks at 14.4° (002), 32.7° (100), 39.5° (103), 49.8° (105), and 58.3° (110) that have been compared to the pure hexagonal MoS₂ with lattice constants $a = 3.160$ and $c = 12.29$ Å (JCPDS no. 37-1492) (Fig. 2b) [34]. No impurity peaks were observed in the XRD pattern, indicating that the sample was highly pure.

The surface morphology of the CPAM-MoS₂ was observed by using SEM and the structure of the NPs was characterized by TEM and high-resolution (HRTEM). The SEM image of the CPAM-MoS₂ powder revealed MoS₂ nanoflakes that overlapped irregularly and curled to form flower-like MoS₂ nanoparticles (Fig. 3a). The TEM image showed the same flower-like structure (Fig. 3b), while the HRTEM image provided a more detailed view (Fig. 3c). The layered structure of the MoS₂ nanoparticles overlapped and the lattice spacing was measured as 0.63 nm, which corresponded to the lattice of (002) planes in a hexagonal MoS₂ structure [34,35]. Furthermore, elemental mapping showed that the elements were well dispersed across the surface of the sample (Fig. 4).

The colloidal stability of CPAM-MoS₂ NPs and MoS₂ NPs were explored using zeta potential and sedimentation volume ratio. The zeta

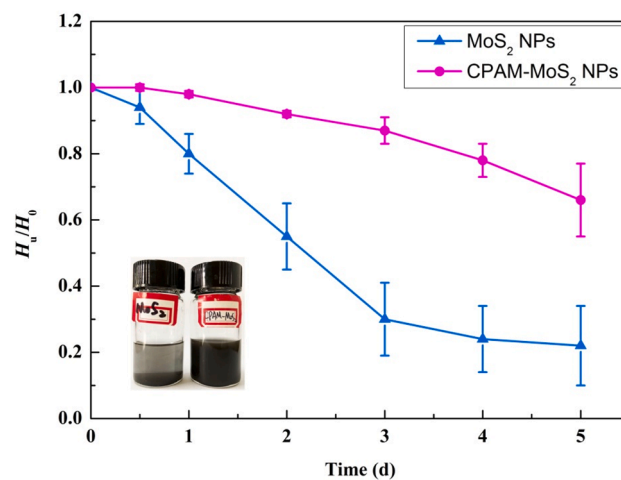


Fig. 5. The colloidal stability of CPAM-MoS₂ NPs: sedimentation volume ratio (H_u/H_0) versus time.

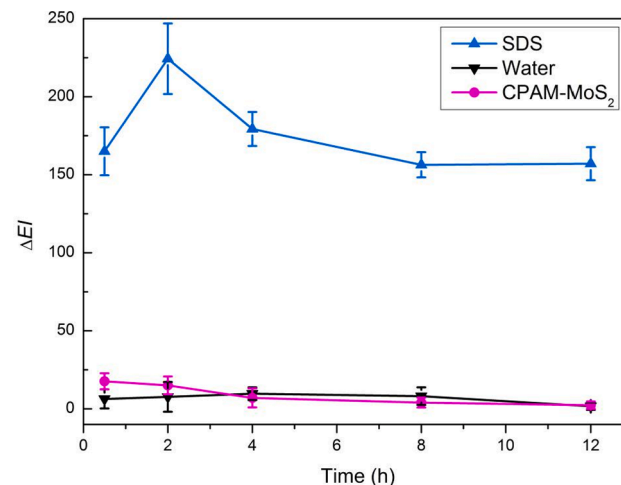


Fig. 6. *In vivo* skin erythema measurement of CPAM-MoS₂ NPs.

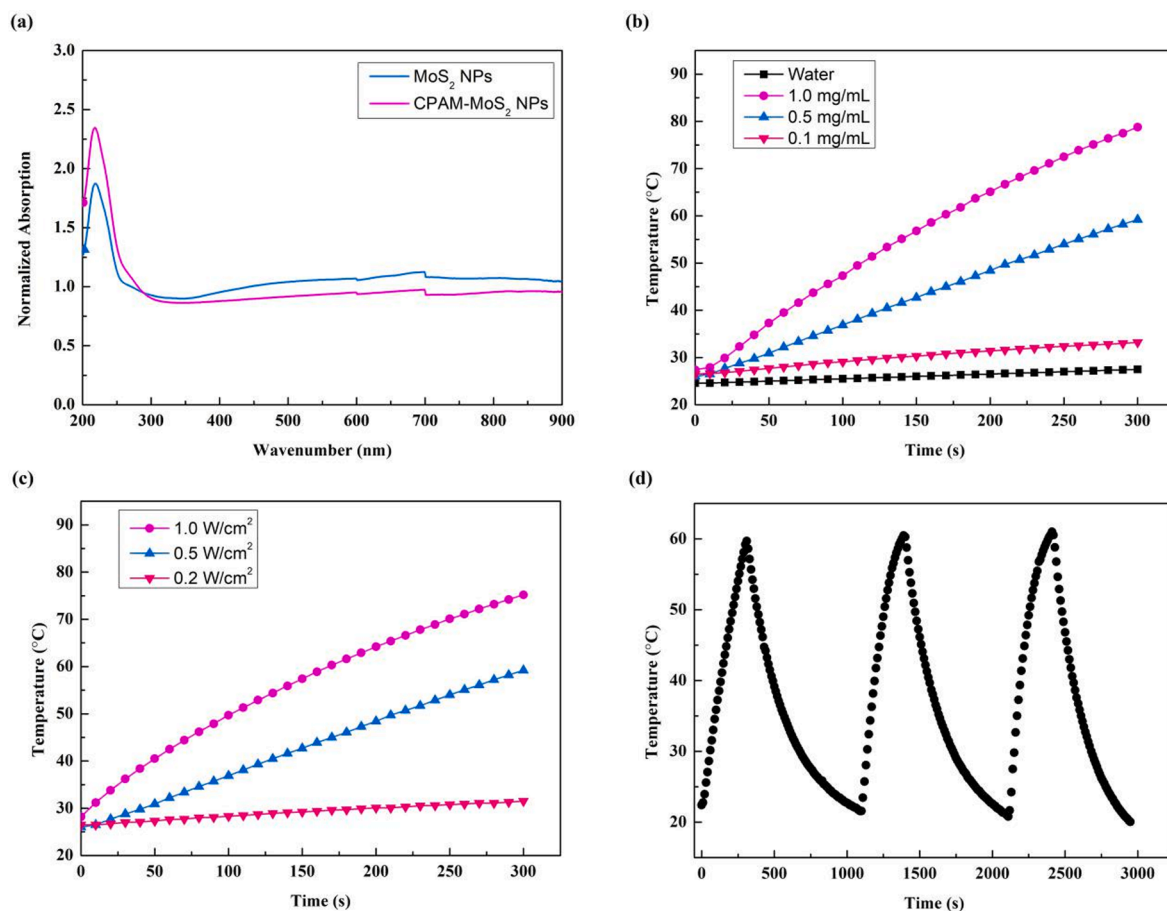


Fig. 7. Photothermal conversion of the CPAM-MoS₂ NPs. (a) UV-vis absorption spectra of MoS₂ and CPAM-MoS₂ NPs solutions. (b) The effect of CPAM-MoS₂ NPs on temperature (0.5 W/cm²). (c) The effect of laser density on temperature (0.5 mg/mL). (d) The stability of the photothermal ability of CPAM-MoS₂ NPs (0.5 W/cm², 0.5 mg/mL).

potential of the MoS₂ NPs and CPAM-MoS₂ NPs was measured to be -14.64 ± 1.72 mV and -24.62 ± 3.74 mV, respectively. The results indicated that the CPAM modification increased the stability of the NPs, which was further confirmed by the sedimentation volume ratio. After 5 days of sedimentation, the H_{10}/H_0 of CPAM-MoS₂ NPs and MoS₂ NPs were 0.66 ± 0.09 and 0.22 ± 0.12 , respectively (Fig. 5). The results were probably related to amide groups in CPAM, which could form hydrogen bond with water. Overall, modifying the surface of the MoS₂ NPs with CPAM made them more stable in water.

3.2. Biocompatibility of CPAM-MoS₂ NPs

The results of *in vivo* skin erythema measurement were shown in Fig. 6. In the group of SDS, ΔEI increased significantly, indicating that the rabbits could respond normally to skin irritants. In contrast, ΔEI in the group of CPAM-MoS₂ NPs did not increase, indicating that CPAM-MoS₂ NPs were non-toxic and non-irritated.

3.3. Photothermal conversion performance

The viability of using the light-stimulated CPAM-MoS₂ NPs as a TDDS was evaluated based on photothermal conversion performance (Fig. 7). Previous studies have found that an 808 nm laser was suitable for the stimulation of MoS₂ NPs without causing photo-damage [21,24,26]. The UV-vis absorbance spectra showed that MoS₂ and CPAM-MoS₂ had a similar strong absorbance from UV to NIR regions, suggesting that the CPAM modification did not change the spectral characteristics of MoS₂. Pure water exhibited no photothermal

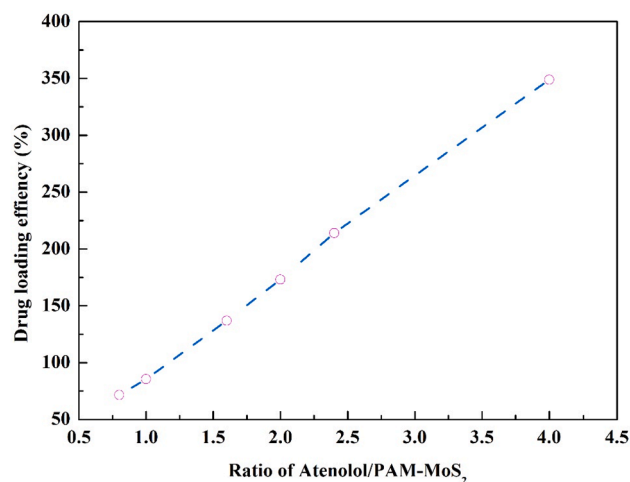


Fig. 8. Drug loading efficiency against the ratios of atenolol to CPAM-MoS₂ NPs.

conversion ability at 808 nm. However, when 1.0 mg/mL CPAM-MoS₂ NPs was added (0.5 W/cm²), the temperature of the solution increased to 78.8 °C in 5 min, indicating the high photo-thermal conversion efficiency of CPAM-MoS₂ NPs. Positive correlations were found between temperature and laser density or the concentration of NPs. In order to avoid skin irritation, the optimised laser density and NPs concentration were 0.5 W/cm² and 0.5 mg/mL, respectively. Moreover, the results

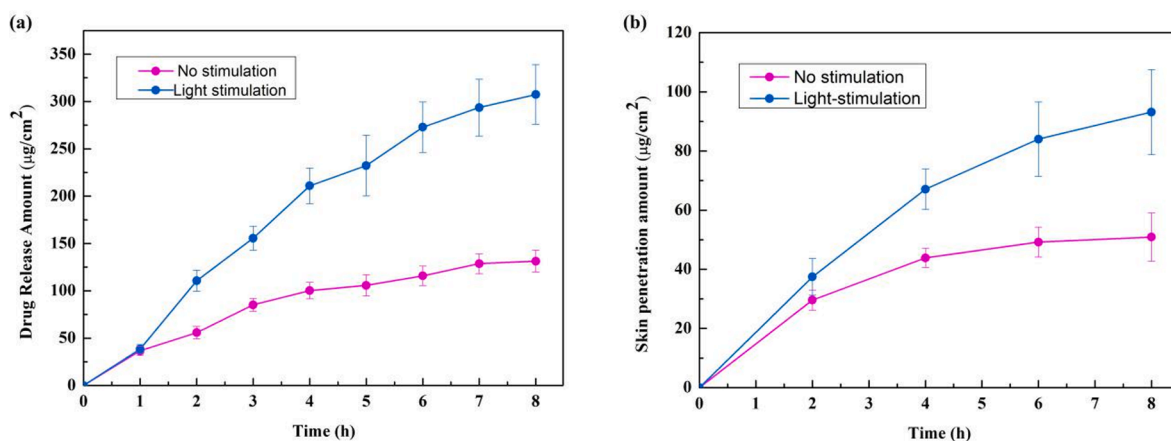


Fig. 9. (a) Drug release from the CPAM-MoS₂ NPs with (blue) and without (pink) light irritation. (b) Skin penetration of atenolol with (blue) and without (pink) light stimulation. (For interpretation of the references to colour in this figure legend, the reader is referred to the web version of this article.)

showed that CPAM modification did not affect the photothermal conversion ability of MoS₂.

3.4. Drug loading

The drug loading efficiency of the CPAM functional MoS₂ Nanoparticles was determined based on the concentration of free drug in solution before and after drug loading. Drug loading efficiency was the ratio of the amount of loaded drug and CPAM-MoS₂ NPs. Drug loading percent was the calculated by the ratio of loaded drug and total drug. The drug loading efficiency increased as the concentration of the atenolol drug increased, where 1 g MoS₂ could load 3.48 ± 0.04 g atenolol at the highest ATE/CPAM-MoS₂ NPs ratio of 4 (Fig. 8). The drug loading percent of $87.2\% \pm 1.12\%$ was achieved at this ratio led to the use of an ATE/CPAM-MoS₂ NPs ratio of 4 in the further experiments.

MoS₂ nanosheets have been widely investigated for cancer treatments [36–38]. However, the multilayer structure of the nanosheets has resulted in poor drug loading efficiency, which was one of biggest limitations in the clinical application of MoS₂ drug delivery systems [39]. The porous structure of the modified CPAM-MoS₂ NPs provided more drug loading sites and increased drug loading efficiency.

3.5. The applicaiton of CPAM-MoS₂ NPs in TDDS

The amount of drug released by the light-stimulated CPAM-MoS₂ NPs was 307.40 ± 31.58 µg/cm², which was significantly increased compared with the control and the enhancement ratio was 2.34 (Fig. 9a). A sudden and significant increase was observed after each light stimulation. The release kinetic constants of CPAM-MoS₂ with or without light stimulation were 2.6 and 1.0, respectively. The results indicated that light stimulation significantly enhanced the release of atenolol from the CPAM-MoS₂ NPs.

The controlled release caused by light stimulation of the CPAM-MoS₂ NPs was further explored by a skin permeation study. Light stimulation resulted in a significant enhancement of skin absorption of atenolol in comparison with the control, and the enhancement ratio was 1.82 ($p < 0.05$) was measured (Fig. 9b). Drug penetration was significantly enhanced immediately after light stimulation, which is important in disease treatment. What's more, dose depletion showed at 4 h in the control group, but had not been shown in the light stimulation group during the whole study, indicating that the light stimulation could not enhanced drug penetration, but also prolong the effect time of TDDS. Skin permeation involves the passive diffusion of the drug across the skin and was facilitated by the increased temperature [40]. The photothermal conversion ability of the CPAM-MoS₂ NPs enhance drug release, and further increased and prolonged atenolol permeation across the

skin.

Polymer-functional inorganic nanomaterials is a popular research topic in drug delivering [41]. In comparison with unmodified inorganic nanomaterials, polymers offer increased flexible structural adjustability and compatibility with various delivery vehicles by adjusting the hydrophilic and hydrophobic balance [42,43]. Functional nanoparticles are widely used in controlled drug release applications. Light is a commonly used stimulus for drug release from nano-platforms [44]. Compared with graphene and gold nanorods, MoS₂ has better photothermal effect. Chou et al. developed a MoS₂-based NIR photothermal agent comprising ce-MoS₂ nanosheets that offered greater photothermal performance than graphene and gold nanorods [21]. The results were further confirmed by our study. Meanwhile, MoS₂-based NPs have higher drug loading rate than graphene oxide. Liu et al. used MoS₂ nanosheets paired with a PEG carrier to load a variety of therapeutic molecules, where the drug loading ratio of the MoS₂ nanosheets was superior to graphene oxide [26]. The CPAM-MoS₂ NPs not only showed better photothermal effect and higher drug loading rate, but also exhibited superior dispersion properties and colloidal stability, which made it possible to apply CPAM-MoS₂ NPs on controlled release.

4. Conclusions

CPAM-MoS₂ NPs were synthesized to serve as a transdermal nano-platform for the treatment of hypertension. The three-dimensional (3D) flower-like CPAM-MoS₂ NPs with large surface area showed huge drug loading percent of 87.2% and extraordinary photothermal conversion ability, which made the developed TDDS controllable, prolonged the treatment time and avoided dose depletion. This is the first application of CPAM-MoS₂ NPs in a TDDS and further *in vivo* studies are recommended to evaluate this novel drug delivery system.

Funding

This research was funded by Liaoning Science and Technology (No. 20180550409), Shenyang medical college of science and technology fund project (No. 20186073) and Specialized Research Fund for Introducing Talents of Hebei Agricultural University (No. YJ201908).

Declaration of Competing Interest

The authors declare that they have no known competing financial interests or personal relationships that could have appeared to influence the work reported in this paper.

References

- [1] A.C. Anselmo, S. Mitragotri, An overview of clinical and commercial impact of drug delivery systems, *J. Control. Release* 190 (2014) 15–28.
- [2] R.M. Hathout, S. Mansour, N.D. Mortada, A.S. Geneidi, R.H. Guy, Uptake of microemulsion components into the stratum corneum and their molecular effects on skin barrier function, *Mol. Pharm.* 7 (2010) 1266–1273.
- [3] A. Ahad, M. Aqil, A. Ali, Investigation of antihypertensive activity of carbopol valsartan transdermal gel containing 1,8-cineole, *Int. J. Biol. Macromol.* 64 (2014) 144–149.
- [4] A. Ahad, M. Aqil, K. Kohli, H. Chaudhary, Y. Sultana, M. Mujeeb, S. Talegaonkar, Chemical penetration enhancers: a patent review, *Expert Opin. Ther. Pat.* 19 (2009) 969–988.
- [5] S. Wiedersberg, R.H. Guy, Transdermal drug delivery: 30+ years of war and still fighting!, *J. Control. Release* 190 (2014) 150–156.
- [6] A. Alexander, S. Dwivedi, T.K. Ajazuddin, S. Giriet, S. Saraf, D.K.T. Saraf, Approaches for breaking the barriers of drug permeation through transdermal drug delivery, *J. Control. Release* 164 (2012) 26–40.
- [7] H.S. Tan, W.R. Pfister, Pressure-sensitive adhesives for transdermal drug delivery systems, *Pharm. Sci. Technol. Today* 2 (1999) 60–69.
- [8] C. Strasinger, K.S. Paudel, J. Wu, D. Hammell, R.R. Pinninti, B.J. Hinds, A. Stinchcomb, Programmable transdermal clonidine delivery through voltage-gated carbon nanotube membranes, *J. Pharm. Sci.* 103 (2014) 1829–1838.
- [9] X. Zhou, Y. Hao, L. Yuan, S. Pradhan, K. Shrestha, O. Pradhan, H. Liu, W. Li, Nanoformulations for transdermal drug delivery: A review, *Chinese Chem Lett.* 29 (2018) 1713–1724.
- [10] A. Zhang, A. Li, W. Zhao, G. Yan, B. Liu, M. Liu, B. Huo, J. Liu, An efficient and self-guided chemo-photothermal drug loading system based on copolymer and transferrin decorated MoS₂ nanodots for dually controlled drug release, *Chem. Eng. J.* 342 (2018) 120–132.
- [11] K. Bhattacharyya, S. Mukherjee, Fluorescent metal nano-clusters as next generation fluorescent probes for cell imaging and drug delivery, *Bull. Chem. Soc. Jpn.* 91 (2018) 447–454.
- [12] B.L. Li, R. Li, H.L. Zou, K. Ariga, N.B. Li, D.T. Leong, Engineered functionalized 2D nanoarchitectures for stimuli-responsive drug delivery, *Mater. Horiz.* 7 (2020) 455–469.
- [13] D. Alba-Molina, J.J. Giner-Casares, M. Cano, Bioconjugated plasmonic nanoparticles for enhanced skin penetration, *Top Curr. Chem.* 8 (2020) 378.
- [14] L.A. Perelman, C. Pacholski, Y.Y. Li, M.S. VanNieuwenhze, M.S. Vannieuwenhze, M. J. Sailor, pH-triggered release of vancomycin from protein-capped porous silicon films, *Nanomedicine* 3 (2008) 31–43.
- [15] Y. Qiu, K. Park, Environment-sensitive hydrogels for drug delivery, *Adv. Drug Del. Rev.* 64 (2012) 49–60.
- [16] X. Luo, X.T. Cui, Electrochemically controlled release based on nanoporous conducting polymers, *Electrochem. Commun.* 11 (2009) 402–404.
- [17] M. Choi, K.-G. Kim, J. Heo, H. Jeong, S.Y. Kim, J. Hong, Multilayered graphene nano-film for controlled protein delivery by desired electro-stimuli, *Sci. Rep.* 5 (2015) 17631.
- [18] A. Kurniawan, S. Muneekaew, C.-W. Hung, S.-H. Chou, M.-J. Wang, Modulated transdermal delivery of nonsteroidal anti-inflammatory drug by macroporous poly(vinyl alcohol)-graphene oxide nanocomposite films, *Int. J. Pharm.* 566 (2019) 708–716.
- [19] Y. Chen, Y. Yang, Y. Xian, P. Singh, J. Feng, S. Cui, A. Carrier, K. Oakes, T. Luan, X. Zhang, Multifunctional graphene-oxide-reinforced dissolvable polymeric microneedles for transdermal drug delivery, *ACS Appl. Mater. Interfaces* 12 (2019) 352–360.
- [20] J. Li, H. Liu, J. Ming, D. Sun, X. Chen, X. Liu, N. Zheng, The biobehavior, biocompatibility and theranostic application of SPNS and Pd@Au nanoplates in rats and rabbits, *Chem. Sci.* 10 (2019) 1677–1686.
- [21] S.S. Chou, B. Kaehr, J. Kim, B.M. Foley, M. De, P.E. Hopkins, J. Huang, C. J. Brinker, V.P. Dravid, Chemically exfoliated MoS₂ as near-infrared photothermal agents, *Angew. Chem. Int. Ed.* 52 (2013) 1–6.
- [22] J. Liu, J. Zheng, H. Nie, H. Chen, B. Li, L. Jia, Co-delivery of erlotinib and doxorubicin by MoS₂ nanosheets for synergetic photothermal chemotherapy of cancer, *Chem. Eng. J.* 381 (2020), 122541.
- [23] X. Dong, W. Yin, X. Zhang, S. Zhu, X. He, J. Yu, J. Xie, Z. Guo, L. Yan, X. Liu, Q. Wang, Z. Gu, Y. Zhao, Intelligent MoS₂ nanotheranostic for targeted and enzyme-/pH-/NIR-responsive drug delivery to overcome cancer chemotherapy resistance guided by PET imaging, *ACS Appl. Mater. Interfaces* 10 (2020) 4271–4284.
- [24] H. Yang, J. Zhao, C. Wu, C. Ye, D. Zou, S. Wang, Facile synthesis of stable colloidal MoS₂ nanoparticles for combined tumor therapy, *Chem. Eng. J.* 351 (2018) 548–558.
- [25] Y. Sun, X. Wu, K. Zhang, Q. Ren, R. Xie, Electrochemiluminescent quaternary Cu-Zn-In-S nanocrystals as a sensing platform: Enzyme-free and sensitive detection of the FLT3 gene based on triple signal amplification, *Biosens. Bioelectron.* 100 (2018) 445–452.
- [26] T. Liu, C. Wang, X. Gu, H. Gong, L. Cheng, X. Shi, L. Feng, B. Sun, Z. Liu, Drug delivery with PEGylated MoS₂ nano-sheets for combined photothermal and chemotherapy of cancer, *Adv. Mater.* 26 (2014) 3433–3440.
- [27] M.H. Qvist, U. Hoeck, B. Kreilgaard, F. Madsen, Release of chemical permeation enhancers from drug-in-adhesive transdermal patches, *Int. J. Pharm.* 231 (2002) 253–263.
- [28] Y. Chen, J. Wang, D. Cun, M. Wang, J. Jiang, H. Xi, H. Cui, Y. Xu, M. Cheng, L. Fang, Effect of unsaturated menthol analogues on the in vitro penetration of 5-fluorouracil through rat skin, *Int. J. Pharm.* 443 (2013) 120–127.
- [29] L. Liu, H. Jiang, J. Dong, W. Zhang, G. Dang, M. Yang, Y. Li, H. Chen, H. Ji, L. Dong, PEGylated MoS₂ quantum dots for traceable and pH-responsive chemotherapeutic drug delivery, *Colloids Surf. B: Biointerfaces* 185 (2020), 110590.
- [30] K. Hu, N. Zhou, Y. Li, S. Ma, Z. Guo, M. Cao, Q. Zhang, J. Sun, T. Zhang, N. Gu, Sliced Magnetic polyacrylamide hydrogel with cell-adhesive microarray interface: a novel multicellular spheroid culturing platform, *ACS Appl. Mater. Interfaces* 8 (2016) 15113–15119.
- [31] K. Prusty, S.K. Swain, Release of ciprofloxacin drugs by nano gold embedded cellulose grafted polyacrylamide hybrid nanocomposite hydrogels, *Int. J. Biol. Macromol.* 126 (2019) 765–775.
- [32] J. Fang, P. Li, X. Lu, L. Fang, X. Lü, F. Ren, A. Strong, Tough, and osteoconductive hydroxyapatite mineralized polyacrylamide/dextran hydrogel for bone tissue regeneration, *Acta Biomater.* 88 (2019) 503–513.
- [33] C.E. Kadow, P.C. Georges, P.A. Janmey, K.A. Beningo, Polyacrylamide hydrogels for cell mechanics: steps toward optimization and alternative uses, *Methods Cell Biol.* 83 (2007) 29–46.
- [34] G. Tang, Y. Wang, W. Chen, H. Tang, C. Li, Hydrothermal synthesis and characterization of novel flowerlike MoS₂ hollow microspheres, *Mater. Lett.* 100 (2013) 15–18.
- [35] X. Zhang, X. Huang, M. Xue, X. Ye, W. Lei, H. Tang, C. Li, Hydrothermal synthesis and characterization of 3D flower-like MoS₂ microspheres, *Mater. Lett.* 148 (2015) 67–70.
- [36] S. Wang, K. Li, Y. Chen, H. Chen, M. Ma, J. Feng, Q. Zhao, J. Shi, Biocompatible PEGylated MoS₂ nanosheets: Controllable bottom-up synthesis and highly efficient photothermal regression of tumor, *Biomaterials* 39 (2015) 206–217.
- [37] M. Xie, N. Yang, J. Cheng, M. Yang, T. Deng, Y. Li, C. Feng, Layered MoS₂ nanosheets modified by biomimetic phospholipids: Enhanced stability and its synergistic treatment of cancer with chemo-photothermal therapy, *Colloids Surf. B: Biointerfaces* 187 (2020), 110631.
- [38] T. Liu, S. Shen, Y. Huang, X. Zhang, Z. Lai, T.H. Tran, Z. Liu, L. Cheng, Controllable growth of Au nanostructures onto MoS₂ nanosheets for dual-modal imaging and photothermal–radiation combined therapy, *Nanoscale* 11 (2019) 22788–22795.
- [39] W. Feng, L. Chen, M. Qin, X. Zhou, Q. Zhang, Y. Miao, K. Qiu, Y. Zhang, C. He, Flower-like PEGylated MoS₂ nanoflakes for near-infrared photothermal cancer therapy, *Sci. Rep.* 5 (2015) 17422.
- [40] W. Song, P. Quan, S. Li, C. Liu, S. Lv, Y. Zhao, L. Fang, Probing the role of chemical enhancers in facilitating drug release from patches: Mechanistic insights based on FT-IR spectroscopy, molecular modeling and thermal analysis, *J. Control. Release* 227 (2016) 13–22.
- [41] R. Liang, M. Wei, D.G. Evans, X. Duan, Inorganic nanomaterials for bioimaging, targeted drug delivery and therapeutics, *Chem. Commun.* 50 (2014) 14071–14081.
- [42] G. Cutrone, J.M. Casas-Solvas, A. Vargas-Berenguel, Cyclodextrin-modified inorganic materials for the construction of nanocarriers, *Int. J. Pharm.* 531 (2017) 621–639.
- [43] R. Liu, S. Liu, J. Yu, W. Zhang, J. Dai, Y. Zhang, G. Zhang, The construction of a hydrophilic inorganic layer enables mechanochemically robust super antifouling UHMWPE composite membrane surfaces, *Polymers* 12 (2020) 569.
- [44] Q. Liu, C. Zhan, D.S. Kohane, Phototriggered drug delivery using inorganic nanomaterials, *Bioconjug. Chem.* 28 (2017) 98–104.